Three-Level Optimized Pulse Patterns for Grid-Connected Converters with LCL Filters

Shirin Rahmanpour
Faculty of Inf. Technol. and Commun. Sciences
Tampere University
Tampere, Finland
shirin.rahmanpour@tuni.fi

Petros Karamanakos
Faculty of Inf. Technol. and Commun. Sciences
Tampere University
Tampere, Finland
p.karamanakos@ieee.org

Tobias Geyer
Motion System Drives
ABB Switzerland Ltd
Turgi, Switzerland
t.geyer@ieee.org

***Abstract*—This paper presents the computation of three-level optimized pulse patterns (OPPs) for converters connected to the grid via LCL filters. To meet the relevant harmonic grid codes, the OPP optimization problem considers the transfer function from the switching function harmonics to the grid current harmonics, while respecting the constraints that relate to the current harmonic limits. Moreover, the proposed problem relaxes the restrictions that are traditionally imposed on the switching signals, i.e., the quarter-wave symmetry and unipolar switch positions. In doing so, the current distortions are less than those of the conventional constrained OPPs, while they are occasionally even lower than those of the OPPs without constraints on the current harmonics. The presented numerical results demonstrate the superior harmonic performance of the computed OPPs compared with conventional modulation techniques, such as space vector modulation (SVM).**

***Index Terms*—Grid-connected converters, grid standards, harmonic distortions, optimized pulse patterns (OPPs), selective harmonic mitigation (SHM), pulse width modulation (PWM).**

I. Introduction

Power electronic systems with power ratings of 1 MVA and above, such as medium-voltage (MV) converters, need to be operated at very low switching frequencies (well below 1 kHz) to keep the switching losses low. Conventional modulation methods, such as carrier-based pulse width modulation (CB-PWM) or space vector modulation (SVM), however, do not perform well at low pulse numbers, i.e., at a low ratio of switching-to-fundamental frequency [1]. To achieve high-quality converter outputs at low pulse numbers, programmed PWM schemes, such as selective harmonic elimination (SHE) and optimized pulse patterns (OPPs), can be employed instead [2], [3], in which the switching patterns are calculated in an offline procedure. Specifically, SHE computes the switching angles (i.e., switching time instants) of the switching patterns by solving a system of nonlinear equations such that specific harmonics are eliminated. As for the switching angles of the OPPs, these are computed by solving an optimization problem that accounts for the output current total demand distortion (TDD) in its objective function.

Despite the above-mentioned advantage of SHE and OPP techniques, when grid-connected converters are of interest, both methods do not fully achieve the desired performance. This is due to the fact that the output current of such converters need to comply with relevant harmonic grid codes, such as the IEEE 519 standard [4], which impose stringent limits on current harmonics and the TDD at the point of common coupling (PCC). Since these codes are meant to prevent the grid customers from harming each other, they are of great importance. To act in accordance with grid standards and reduce the harmonics injected to the grid, the power converters are typically connected to the grid through harmonic filters, most commonly LCL filters. Such filters, however, even though they attenuate the high-order harmonics, are not that effective with low-order harmonics, implying that respecting the grid standards is not trivial.

To address—at least partly—this challenge and abide by the grid codes, SHE can be modified to mitigate the effect of noneliminated harmonics. To this aim, the so-called selective harmonic mitigation (SHM) methods suggested in [5] and [6] for grid-connected converters adjust the dc-link voltage, i.e., the modulation index. In doing so, however, these techniques drastically limit the operational range of the converter. In [7] and [8], the proposed SHM methods compute the switching angles by minimizing the difference between selected harmonic amplitudes and their maximum allowed levels imposed by the harmonic grid standards. This strategy improves the harmonic performance of the grid current, but alas, it requires a high number of pulses to meet the harmonic grid codes. This renders this approach unsuitable for MV applications. Moreover, the grid current TDD, although below the value required by the harmonic grid codes, remains relatively high, especially at higher modulation indices.

In contrast to the SHE/SHM techniques employed in the aforementioned works, OPPs show better harmonic performance as they are computed such that entire harmonic content of the switching signal is minimized [9]. However, OPPs, similarly to SHE/SHM methods, are computed for first-order systems—typically by assuming an inductive load—thus their benefits can be compromised when used with higher-order systems, such as converters with LCL filters.[1] When OPPs, however, are tailored to higher-order systems, then they can produce the lowest possible grid current TDD at low switching frequencies, as shown in [10]. Nevertheless, the OPPs in

[1] In practice, for MV applications, the three-level converter is connected to the grid via an LC filter and a transformer, giving rise to an LCL configuration.

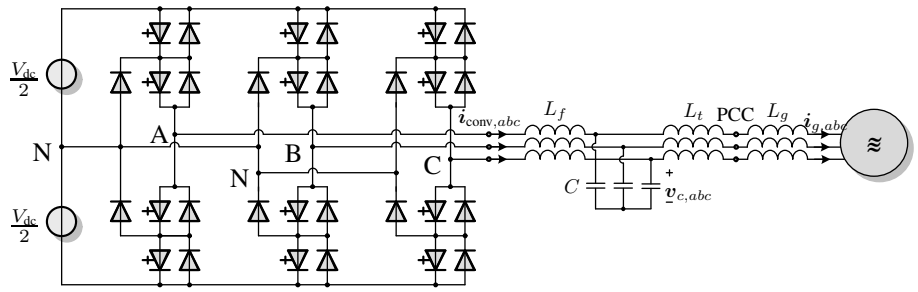

Fig. 1. Graphical representation of the three-level NPC converter connected to the grid via an LCL filter.

that work do not guarantee that specific harmonic limits are fulfilled as only the current TDD is considered in the optimization process.

Motivated by the above, this paper proposes a method to compute three-level OPPs for grid-connected converters with LCL filter that meet the relevant grid standards. To do so, the OPP optimization problem is reformulated by taking the transfer function from the switching function to the grid current into account. Furthermore, additional constraints are included in the optimization problem to ensure that the current harmonics that would otherwise violate their limits are kept below them. In addition, to mitigate the expected increase in the current TDD resulting from the harmonic limitations, the restrictions that are typically imposed on the symmetry and polarity of the switch positions are relaxed to increase the solution search space. As demonstrated by the numerical results, the computed constrained OPPs with relaxed properties produce currents that comply with the harmonic grid codes. Moreover, the presented OPPs not only exhibit significantly better harmonic performance compared with conventional modulation methods, such as space vector modulation (SVM), but also achieve current TDDs that can occasionally be even lower than those of the unconstrained conventional OPPs.

II. OPPs for Grid-Connected Converters with LCL Filters

The computation of OPPs is done for an MV power electronic system consisting of a three-level neutral-point-clamped (NPC) voltage-source converter that is connected to the grid via an LCL filter, see Fig. 1. In the sequel of this section, the model of this system used in the OPP optimization problem as well as the subsequent computation of OPPs—without and with relaxed symmetry and polarity properties—that meet the harmonic grid standards are presented.

A. Modeling of the Grid-Connected Converter System

Consider the (reduced) Clarke transformation $\boldsymbol{\xi}_{\alpha\beta} = \boldsymbol{K}\boldsymbol{\xi}_{abc}$ that maps quantities $\boldsymbol{\xi}_{abc} = [\xi_a\ \xi_b\ \xi_c]^T$ from the three-phase (abc) plane to quantities $\boldsymbol{\xi}_{\alpha\beta} = [\xi_\alpha\ \xi_\beta]^T$ in the stationary, orthogonal ($\alpha\beta$) plane via the matrix

$$\boldsymbol{K} = \frac{2}{3}\begin{bmatrix} 1 & -\frac{1}{2} & -\frac{1}{2} \\ 0 & \frac{\sqrt{3}}{2} & -\frac{\sqrt{3}}{2} \end{bmatrix}.$$

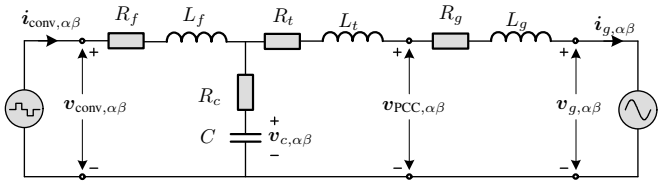

Fig. 2. Equivalent circuit of the converter system in the $\alpha\beta$-plane

The differential equations that characterize the system under consideration can be derived by applying circuit analysis to the equivalent circuit of the system in the $\alpha\beta$ plane, see Fig. 2. This yields [11][2]

$$L_f \frac{{\rm d}\boldsymbol{i}_{\rm conv}(t)}{{\rm d}t} = -R_1\boldsymbol{i}_{\rm conv}(t) + R_c\boldsymbol{i}_g(t) - \boldsymbol{v}_c(t) + \boldsymbol{v}_{\rm conv}(t)\,, \quad \text{(1a)}$$

$$L_{gt} \frac{{\rm d}\boldsymbol{i}_g(t)}{{\rm d}t} = R_c\boldsymbol{i}_{\rm conv}(t) - R_2\boldsymbol{i}_g(t) + \boldsymbol{v}_c(t) - \boldsymbol{v}_g(t)\,, \quad \text{(1b)}$$

$$\frac{{\rm d}\boldsymbol{v}_c(t)}{{\rm d}t} = \frac{1}{C}\boldsymbol{i}_{\rm conv}(t) - \frac{1}{C}\boldsymbol{i}_g(t)\,, \quad \text{(1c)}$$

$$\frac{{\rm d}\boldsymbol{v}_g(t)}{{\rm d}t} = \begin{bmatrix} o & -\omega_g \\ \omega_g & 0 \end{bmatrix}\boldsymbol{v}_g(t)\,, \quad \text{(1d)}$$

where the converter voltage is obtained through

$$\boldsymbol{v}_{\rm conv}(t) = \frac{V_{\rm dc}}{2}\boldsymbol{K}\boldsymbol{u}_{abc}(t)\,, \quad (2)$$

with $V_{\rm dc}$ being the dc-link voltage of the converter, and $\boldsymbol{u}_{abc} = [u_a\ u_b\ u_c]^T \in \{-1, 0, 1\}^3$ the three-phase switch position. Moreover, the system parameters shown in (1) comprise the lumped inductance $L_{gt} = L_g + L_t$, which combines the inductances of the grid L_g and transformer L_t. In addition, $R_1 = R_f + R_c$ comprises the series resistances of the filter inductance L_f and capacitance C, respectively, while the resistances of the grid and transformer, i.e., R_g and R_t, respectively, are considered in $R_2 = R_c + R_g + R_t$. Finally, ω_g is the angular frequency of the grid.

To describe the dynamics of the grid-connected converter system, the state vector $\boldsymbol{x}$ is chosen to comprise the converter current $\boldsymbol{i}_{{\rm conv},\alpha\beta}$, grid current $\boldsymbol{i}_{g,\alpha\beta}$, capacitor voltage $\boldsymbol{v}_{c,\alpha\beta}$, and grid voltage $\boldsymbol{v}_{g,\alpha\beta}$, i.e., $\boldsymbol{x} = [\boldsymbol{i}_{{\rm conv},\alpha\beta}^T\ \boldsymbol{i}_{g,\alpha\beta}^T\ \boldsymbol{v}_{c,\alpha\beta}^T\ \boldsymbol{v}_{g,\alpha\beta}^T]^T \in \mathbb{R}^8$. Moreover, by defining the three-phase switch position $\boldsymbol{u}_{abc}$ as the input to the system,

[2]Note that in (1), the $\alpha\beta$ subscript is dropped from the respective variables for convenience, whereas abc variables have their subscript explicitly stated.

and choosing the grid current as the system output, i.e., $\boldsymbol{y} = \boldsymbol{i}_{g,\alpha\beta} \in \mathbb{R}^2$, the state-space model of the system can be obtained from (1) as follows

$$\begin{aligned} \frac{\mathrm{d}\boldsymbol{x}(t)}{\mathrm{d}t} &= \boldsymbol{A}\boldsymbol{x}(t) + \boldsymbol{B}\boldsymbol{u}_{abc}(t)\,, \\ \boldsymbol{y}(t) &= \boldsymbol{C}\boldsymbol{x}(t)\,, \end{aligned} \tag{3}$$

with the state-space matrices

$$\boldsymbol{A} = \begin{bmatrix} -\frac{R_1}{L_f}\boldsymbol{I}_2 & \frac{R_c}{L_f}\boldsymbol{I}_2 & -\frac{1}{L_f}\boldsymbol{I}_2 & \boldsymbol{0}_2 \\ \frac{R_c}{L_{gt}}\boldsymbol{I}_2 & -\frac{R_2}{L_{gt}}\boldsymbol{I}_2 & \frac{1}{L_{gt}}\boldsymbol{I}_2 & -\frac{1}{L_{gt}}\boldsymbol{I}_2 \\ \frac{1}{C}\boldsymbol{I}_2 & -\frac{1}{C}\boldsymbol{I}_2 & \boldsymbol{0}_2 & \boldsymbol{0}_2 \\ \boldsymbol{0}_2 & \boldsymbol{0}_2 & \boldsymbol{0}_2 & \begin{bmatrix} 0 & -\omega_g \\ \omega_g & 0 \end{bmatrix} \end{bmatrix},$$

$$\boldsymbol{B} = \frac{V_{\mathrm{dc}}}{2L_f}\begin{bmatrix} \boldsymbol{I}_2 \\ \boldsymbol{0}_2 \\ \boldsymbol{0}_2 \\ \boldsymbol{0}_2 \end{bmatrix}\boldsymbol{K}, \quad \boldsymbol{C} = \begin{bmatrix} \boldsymbol{0}_2 & \boldsymbol{I}_2 & \boldsymbol{0}_2 & \boldsymbol{0}_2 \end{bmatrix}.$$

Here, $\boldsymbol{I}_2$ and $\boldsymbol{0}_2$ denote the identity and zero matrices of dimension two, respectively.

With (3), the transfer matrix from the system input (the converter switch position $\boldsymbol{u}_{abc}$) to the system output (the grid current $\boldsymbol{i}_{g,\alpha\beta}$), i.e., $\boldsymbol{H}(s) = \mathcal{L}\{\boldsymbol{i}_{g,\alpha\beta}\}(s)/\mathcal{L}\{\boldsymbol{u}_{abc}\}(s)$, is derived. This matrix is employed to map the effect of the applied pulse pattern on the grid current, as shown in the next section.

B. Three-Level OPPs Considering the LCL Filter

Assuming three-phase symmetry, it suffices to compute offline the three-level switching signal $u_a \equiv u(\theta)$ for phase a, as u_b and u_c can be obtained by phase-shifting u_a by $-2\pi/3$ and $2\pi/3$, respectively. In addition, it is common practice to impose quarter- and half-wave symmetry (QaHWS) on the 2π-periodic signal $u(\theta)$, i.e., $u(\pi - \theta) = u(\theta)$ and $u(\pi + \theta) = -u(\theta)$, respectively. Furthermore, only non-negative switch positions are typically considered in the positive half-wave of the fundamental period. As a result, the switching signal can be fully characterized by d switching angles $\alpha_i \in [0, \pi/2]$, $i \in \{1, \ldots, d\}$, and $d+1$ switch positions $u_i \in \{0, 1\}$, $i \in \{0, \ldots, d\}$, in the first quarter of the fundamental period, while the initial switch position u_0 is zero. The pulse number d represents the number of switching transitions $\Delta u_i = u_i - u_{i-1} \in \{-1, 1\}$ in the QaHWS switched waveform within $[0, \pi/2]$. Note that switching by more than one level up or down is prohibited for multilevel converters owing to the risk of a short circuit [12]. Moreover, for QaHWS OPPs with unipolar switch positions, the switching transitions become $\Delta u_i = (-1)^{i+1}$, $i \in \{1, \ldots, d\}$.

Given the above, the periodic switching signal $u(\theta)$ can be represented by the following Fourier series expansion [13]

$$\begin{aligned} u(\theta) &= \sum_{n=1,3,5,7,\ldots} \left(a_n \cos(n\theta) + b_n \sin(n\theta)\right) \\ &= \sum_{n=1,3,5,7,\ldots} b_n \sin(n\theta)\,, \end{aligned} \tag{5}$$

with

$$b_n = \hat{u}_n = \frac{4}{n\pi}\sum_{i=1}^{d} \Delta u_i \cos(n\alpha_i)\,,$$

where $\hat{u}_n$ denotes the amplitude of the n^{th} harmonic of the single-phase pulse pattern. Therefore, the amplitude of the corresponding voltage harmonic is $\hat{v}_n = (V_{\mathrm{dc}}/2)\,\hat{u}_n$. Note that due to the half-wave symmetry (HWS) of $u(\theta)$ only odd harmonics appear in (5). Moreover, QaHWS implies that the only the b_n Fourier coefficients are considered, while all the a_n coefficients are zero. For details on the derivation of the Fourier coefficients when imposing different symmetry conditions, the interested reader is referred to [13].

The harmonic components of the switched converter voltage cause current harmonic distortions which adversely affect the load. To quantify the quality of the current, its TDD is adopted as a relevant performance metric, i.e.,

$$I_{\mathrm{TDD}} = \frac{1}{\sqrt{2}I_{\mathrm{nom}}}\sqrt{\sum_{n\neq 1} \hat{i}_n^2}\,, \tag{6}$$

where I_{nom} is the rms value of the nominal current, and $\hat{i}_n$ the amplitude of the n^{th} harmonic of the current of interest. Focusing on the grid current, the amplitude of its n^{th} harmonic $\hat{i}_{g,n}$ is related to the amplitude of the n^{th} harmonic of the switched waveform $\hat{u}_n$ through the gain g_n that can be computed by replacing s with $\jmath n\omega_1$ in the transfer matrix $\boldsymbol{H}(s)$ obtained from (3) (see Section II-A), where ω_1 is the angular fundamental frequency. Therefore, the grid current TDD is

$$I_{\mathrm{TDD}} = \underbrace{\frac{\sqrt{2}V_{\mathrm{dc}}}{\pi I_{\mathrm{nom}}}}_{c}\sqrt{\sum_{n=5,7,\ldots}\left(\frac{g_n}{n}\sum_{i=1}^{d}\Delta u_i\cos(n\alpha_i)\right)^2}\,. \tag{7}$$

Note that the triplen current harmonics are not considered in (7) since the triplen voltage harmonics ($n = 3, 9, 15, \ldots$) do not drive harmonic current in a balanced three-phase system.

The current TDD in (7) can be interpreted as $I_{\mathrm{TDD}} = c\sqrt{J}$ in which the constant c depends only on the system parameters. By discarding the constant—and thus irrelevant—scaling factor c, the OPPs that produce the minimum grid current I_{TDD}, while accounting for the LCL filter, can be computed by minimizing J, which is chosen as the objective function of the proposed OPP optimization problem. To this end, the following nonconvex optimization problem is solved over the whole range of modulation indices $m \in [0, 4/\pi]$

$$\underset{\boldsymbol{\alpha}_Q=[\alpha_1\ \ldots\ \alpha_d]^T}{\text{minimize}} \quad \sum_{n=5,7,\ldots}\left(\frac{g_n}{n}\sum_{i=1}^{d}\Delta u_i\cos(n\alpha_i)\right)^2 \tag{8a}$$

$$\text{subject to} \quad b_1 = \frac{4}{\pi}\sum_{i=1}^{d}\Delta u_i\cos(\alpha_i) = m \tag{8b}$$

$$0 \le \alpha_1 \le \alpha_2 \le \ldots \le \alpha_d \le \frac{\pi}{2} \tag{8c}$$

$$\Delta u_i = (-1)^{i+1} \ \ \forall i \in \{1, \ldots, d\}. \tag{8d}$$

Note that the switching angles α_i in the first quarter of the fundamental period are the only optimization variables when QaHWS and unipolar switch positions are considered. In (8), constraint (8b) ensures that the desired modulation index m is synthesized, while the $d+1$ inequality constraints (8c) guarantee that the switching angles are in ascending order. It is important to stress that owing to the inclusion of the gain g_n in the objective function (8a), problem (8) enables the computation of OPPs for higher-order systems, such as the one considered in this work (see Fig. 1). This is in stark contrast to the conventional formulation of the OPP problem, where the objective function is suitable only for the first-order systems since an inductive load is typically assumed [13].

C. Constrained OPPs that Meet the Harmonic Grid Standards

Even though the OPPs computed by solving (8) produce the minimum grid current TDD, they do not ensure that individual current harmonics do not exceed the limits imposed by the relevant grid standards. To address this, the OPP optimization problem (8) is modified by adding constraints of the form

$$\hat{u}_n \leq \frac{1}{g_n}\frac{2}{V_{\text{dc}}}\hat{i}_{n,\max} \tag{9}$$

so that the current harmonics are limited to their desired levels. Constraint (9) maps the limit on the amplitude of the n^{th} current harmonic $\hat{i}_{n,\max}$, as dictated by the grid standards [4], to the switching signal harmonic via the gain g_n. Hence, by solving problem (8) when augmented with constraint (9), the aim is to achieve the lowest possible grid current TDD while meeting the harmonic limits imposed by the grid standards as well as possible. To this aim, the constraints (9) are imposed on the low-order non-triplen odd harmonics (e.g., up to the 25^{th} harmonic), as harmonics at higher frequencies are effectively attenuated by the filter. It should be pointed out, however, that due to fact that the harmonic constraints are implemented as hard constraints, the feasibility of the constrained OPP problem is not guaranteed, as also discussed in Section III. This issue can be overcome by, e.g., employing soft constraints, albeit at the expense of small constraint violations.

D. Relaxed OPP Optimization Problem for Grid-Connected Converters

As recently shown in [13], relaxing symmetry and switching restrictions increases the search space of the three-level OPP optimization problem. In other words, the degrees of freedom in the computation process are higher due to the increased domain of the switching angles as well as the additional feasible switching sequences. With regards to the former, by dropping the quarter-wave symmetry, only HWS OPPs are considered, meaning that $2d$ switching angles $\alpha_i \in [0,\pi], i \in \{1,\dots,2d\}$, need to be computed in one half-wave of the fundamental period, as opposed to the d switching angles calculated for QaHWS OPPs. Moreover, considering both positive and negative switch positions in the positive half-wave of the fundamental period and not having strictly $u_0 = 0$, i.e., allowing multipolar switch positions, give rise to more than one candidate pulse pattern, i.e., $2^{d+1}-2$ feasible switching sequences [13]. Hence, when the OPP optimization problem is solved considering HWS and multipolar switch positions, not only $2d$ switching angles need to be computed, but also $2d$ switch positions $u_i \in \{-1,0,1\}, i \in \{0,\dots,2d-1\}$. Note that owing to the imposed HWS the final switch position should be $u_{2d} = -u_0$.

Considering HWS, both Fourier coefficients a_n and b_n are nonzero for the odd harmonics. Thus, the HWS pulse patterns can be represented as follows [13]

$$u(\theta) = \sum_{n=1,3,5,7,\dots} \left(a_n \cos(n\theta) + b_n \sin(n\theta)\right), \tag{10}$$

with

$$a_n = -\frac{2}{n\pi}\sum_{i=1}^{2d} \Delta u_i \sin(n\alpha_i),$$

$$b_n = \frac{2}{n\pi}\sum_{i=1}^{2d} \Delta u_i \cos(n\alpha_i),$$

and $\hat{u}_n = \sqrt{a_n^2 + b_n^2}$ being the amplitude of the n^{th} harmonic of the switching signal.

With the above, and by following the analysis presented in Section II-B, the current TDD resulting from HWS OPPs is given by

$$I_{\text{TDD}} = \underbrace{\frac{V_{\text{dc}}}{\sqrt{2}\pi I_{\text{nom}}}}_{c}\left(\sum_{n=5,7,\dots}\left(\frac{g_n}{n}\right)^2\left(\left(\sum_{i=1}^{2d}\Delta u_i \sin(n\alpha_i)\right)^2 + \left(\sum_{i=1}^{2d}\Delta u_i \cos(n\alpha_i)\right)^2\right)\right)^{1/2}. \tag{11}$$

Considering the part of the current TDD in (11) that is a function of the optimization variables, namely the switching angles $\boldsymbol{\alpha}_H = [\alpha_1 \ \dots \ \alpha_{2d}]^T$ and switch positions $\boldsymbol{u}_H = [u_0 \ \dots \ u_{2d-1}]^T$, the *harmonic-constrained* three-level OPP optimization problem with HWS and multipolar switch positions is formulated as follows

$$\underset{\boldsymbol{\alpha}_H, \boldsymbol{u}_H}{\text{minimize}} \quad J(\boldsymbol{\alpha}_H, \boldsymbol{u}_H) \tag{12a}$$

$$\text{subject to} \quad b_1 = \frac{2}{\pi}\sum_{i=1}^{2d}\Delta u_i \cos(\alpha_i) = m \tag{12b}$$

$$a_1 = -\frac{2}{\pi}\sum_{i=1}^{2d}\Delta u_i \sin(\alpha_i) = 0 \tag{12c}$$

$$0 \leq \alpha_1 \leq \alpha_2 \leq \dots \leq \alpha_{2d} \leq \pi \tag{12d}$$

$$\hat{u}_n \leq \frac{1}{g_n}\frac{2}{V_{\text{dc}}}\hat{i}_{n,\max} \tag{12e}$$

$$u_i \in \{-1,0,1\} \ \forall i \in \{0,\dots,2d-1\} \tag{12f}$$

$$\Delta u_i \in \{-1,1\} \ \forall i \in \{1,\dots,2d\}, \tag{12g}$$

where (12c) is imposed to ensure that the initial phase of the

TABLE I
PARAMETERS OF THE FILTER AND GRID.

Parameter	Symbol	SI value
Filter inductance	L_f	$0.35\,\text{mH}$
Filter resistance	R_f	$0.3\,\text{m}\Omega$
Filter capacitance	C	$420\,\mu\text{F}$
Filter capacitor resistance	R_c	$4\,\text{m}\Omega$
Transformer inductance	L_t	$526.41\,\mu\text{H}$
Transformer resistance	R_t	$16.54\,\text{m}\Omega$
Grid inductance	L_g	$349.19\,\mu\text{H}$
Grid resistance	R_g	$10.97\,\text{m}\Omega$

fundamental component of the OPP is zero. It is noteworthy that problem (12) is not only nonconvex (like (8)), but also mixed-integer due to the multiple candidate pulse patterns. Hence, the optimal switching angles are computed for each candidate pulse pattern, and subsequently the pair of switching angles $\boldsymbol{\alpha}_H$ and switch positions $\boldsymbol{u}_H$ that results in the globally lowest I_{TDD} is chosen as the optimal one.

III. NUMERICAL RESULTS

This section presents the performance of three types of OPPs, namely (a) conventional (i.e., unipolar QaHWS) OPPs, i.e., OPPs computed with (8), (b) current harmonic-constrained unipolar QaHWS OPPs, i.e., OPPs computed with (8) that is augmented with constraint (9), and (c) current harmonic-constrained multipolar HWS OPPs, OPPs obtained by solving problem (12). All the above-mentioned OPPs are computed for the three-level NPC MV converter connected to the grid via an LCL filter, see Fig. 1. The converter has $9\,\text{MVA}$ rated power, a dc-link voltage of $4.84\,\text{kV}$, and a nominal frequency of $50\,\text{Hz}$, while the short-circuit ratio is 15. Moreover, the rated line-to-line grid voltage is $3.15\,\text{kV}$. Finally, according to the parameters provided in Table I, a filter resonance frequency of $491\,\text{Hz}$ results.

Considering $d = 5$, the aforementioned OPP problems are solved for 256 modulation indices in the equidistantly gridded interval $[0, 4/\pi]$. Each optimization problem is solved for 500 random initial points to increase the probability of finding the global minimum. Moreover, the infinite sum of harmonics in the objective functions is approximated by considering the first 500 harmonics as the amplitudes of the current harmonics are very small at higher frequencies.

A. Optimal Switching Angles and Grid Current TDD

The d optimal switching angles resulted from solving (8), i.e., the conventional OPP problem, are depicted in Fig. 3(a). Moreover, Fig. 3(b) shows the d angles obtained when solving (8) with constraint (9) imposed on the first eight odd, non-triplen grid current harmonics (i.e., up to the 25^{th} harmonic). Finally, by using the same constraints for the current harmonics as in the second problem, the $2d$ switching angles of the relaxed (i.e., HWS multipolar) OPP optimization problem (12) are shown in Fig. 3(c).

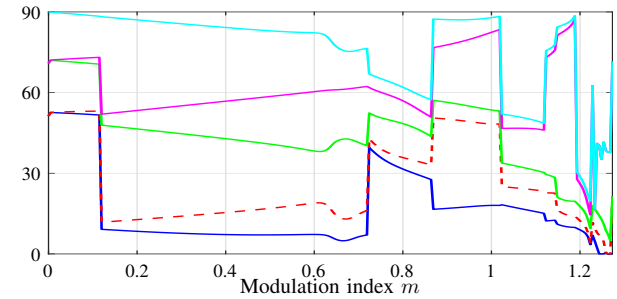

(a) QaHWS unipolar OPPs without constraints on the current harmonics

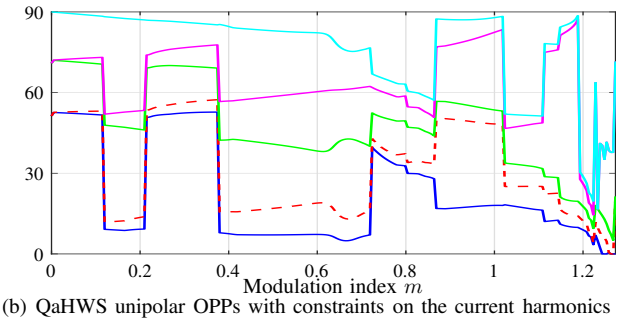

(b) QaHWS unipolar OPPs with constraints on the current harmonics

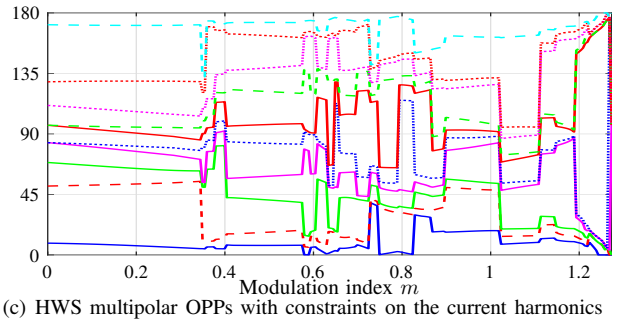

(c) HWS multipolar OPPs with constraints on the current harmonics

Fig. 3. Primary switching angles α_i (degrees) resulted from the unipolar QaHWS OPP optimization problem (a) without and (b) with constraints on the grid current harmonics, and (c) the current harmonic-constrained HWS multipolar OPP optimization problem.

Furthermore, the comparison between the grid current TDDs of the three aforementioned OPP problems is illustrated in Fig. 4 over the entire range of modulation indices $[0, 4/\pi]$. As can be seen, when the harmonics are constrained, the corresponding OPPs have higher current TDDs than for the conventional (i.e., unconstrained) OPPs. The reason for this is that the introduction of constraints on individual current harmonics compromises the optimality of the unconstrained problem, and as a result the current TDD increases. However, the current TDD produced by both types of harmonic-constrained OPPs is still considerably lower than the 5% limit imposed by the grid standards as long as $m < 1.22$. More importantly, the OPPs obtained with the proposed problem (see (12)), i.e., the constrained OPPs with relaxed symmetry and polarity properties, not only produce lower current TDDs than those of the constrained QaHWS unipolar OPPs over the whole range of modulation indices, but they also outperform—in terms of I_{TDD}—the conventional OPPs for some intervals of modulation indices, see Fig. 4. This is thanks to the additional degrees of freedom in problem (12) as it can choose the optimal solution among several pulse patterns and distribute

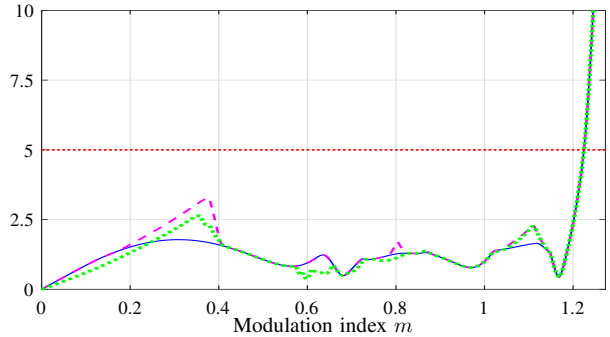

Fig. 4. Current TDD (%) of the QaHWS unipolar OPPs without (solid, blue line) and with (dashed, magenta line) constraints on the grid current harmonics as well as of the harmonic-constrained HWS multipolar OPPs (dotted, green line). The maximum level of current TDD allowed by the grid standards is shown with the dotted red line.

$2d$ switching angles over a wider range of values.

Finally, it is worth discussing the feasibility issue mentioned in Section II-C. As can be seen in Fig. 4, the optimization problems for both harmonic-constrained types of OPPs return current TDDs that exceed the 5% limit when $m \geq 1.22$. This indicates that the harmonic distortions increases significantly at such high modulation indices, implying that the computed OPPs cannot respect the (hard) constraints imposed on individual harmonics. This leads to feasibility issues that cannot be addressed with the presented formulation. Nevertheless, as mentioned in Section II-C, soft constraints can help overcome this issue and enable the optimizer to return feasible (but not necessarily favorable) solutions.

B. Pulse Patterns

Considering that grid-connected converters are typically operated between $m = 1$ and 1.1, the three discussed types of OPPs are presented in this section for modulation indices $m = 1.035$ and $m = 1.085$, see Figs. 5 and 6, respectively. The QaHWS unipolar OPPs—regardless of the presence of harmonic constraints—have a unique sequence of switch positions, i.e., $\boldsymbol{u}_Q = [0\ 1\ 0\ 1 \ldots]^T$, while, as expected, they exhibit QaHWS, see the first two figures of Figs. 5 and 6. On the other hand, when solving (12), HWS OPPs result, as can be seen in Figs. 5(c) and 6(c). However, even though (12) makes it possible to consider different switching sequences for each modulation index, the unipolar sequence is chosen as the optimal one for both examined operating points. It should be mentioned, nevertheless, that multipolar patterns are chosen for a wide range of modulation indices when m is smaller, i.e., for $m \in [0, 0.4] \cup [0.58, 0.66) \cup [0.7, 0.73) \cup [0.75, 0.83)$.

C. Grid Current Harmonics

To provide more insight into the computed OPPs, this section presents the grid current harmonic spectra produced by the three different types of OPPs. The same operating points are considered as in Section III-B. More specifically, the harmonic spectrum of the grid current produced by QaHWS unipolar OPPs without additional constraints (i.e., those computed with (8)) is depicted in Figs. 7(a) and 8(a) for modulation indices $m = 1.035$ and $m = 1.085$, respectively. Owing

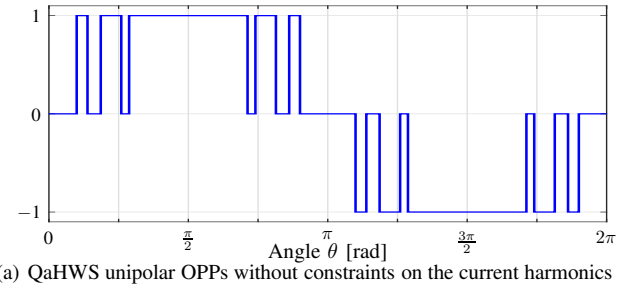

(a) QaHWS unipolar OPPs without constraints on the current harmonics

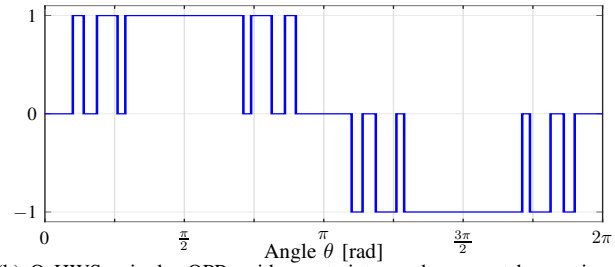

(b) QaHWS unipolar OPPs with constraints on the current harmonics

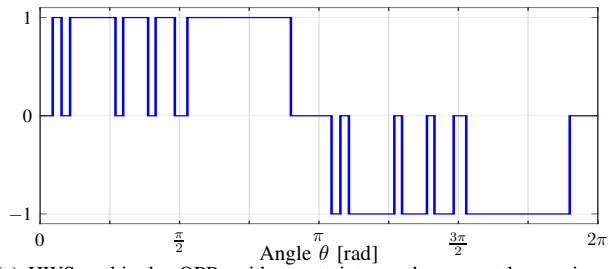

(c) HWS multipolar OPPs with constraints on the current harmonics

Fig. 5. OPPs with $d = 5$ and $m = 1.035$ resulted from the unipolar QaHWS OPP optimization problem (a) without and (b) with constraints on the grid current harmonics, and (c) the current harmonic-constrained HWS multipolar OPP optimization problem.

to the fact that the OPPs are computed by minimizing the current TDD instead of individual harmonics, the harmonic amplitudes are very low. As a result, the current TDDs are as low as $I_{\text{TDD}} = 1.41\%$ and $I_{\text{TDD}} = 1.56\%$, respectively, i.e., much lower than the 5% limit dictated by the IEEE 519 standard [4].[3] Nevertheless, when comparing the amplitude of individual harmonics with their limits imposed by the grid standards, it is observed that the 17^{th} harmonic exceeds its maximum allowed level for both considered modulation indices, see Figs. 7(a) and 8(a).

To reduce the amplitudes of the above-mentioned current harmonics so that they fulfill the harmonic grid standards, the OPPs are computed again by adding constraints of the form (9) to the optimization problem (8) for $n = 5, 7, 11, \ldots, 25$. The resulting grid current spectra clearly demonstrate that the 17^{th} harmonic is now within its limit for both modulation indices, see Fig. 7(b) and Fig. 8(b). Noteworthy, these limitations do not compromise the overall current quality much as the new values of the grid current TDD are 1.42% and 1.93% for $m = 1.035$ and $m = 1.085$, respectively, i.e., still much lower than the $5\,\%$ required by the grid codes. This is attributed to the

[3]Note that the flexibility of the proposed harmonic-constrained OPP optimization problem allows for the adoption of any other grid standards as only the harmonic limits would need to be adjusted.

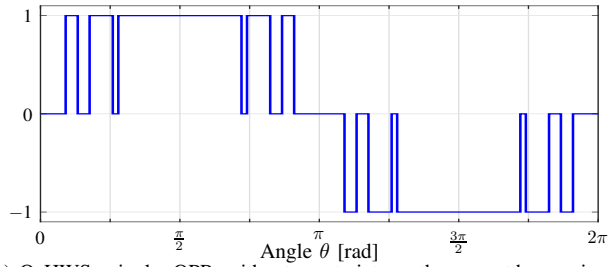

(a) QaHWS unipolar OPPs without constraints on the current harmonics

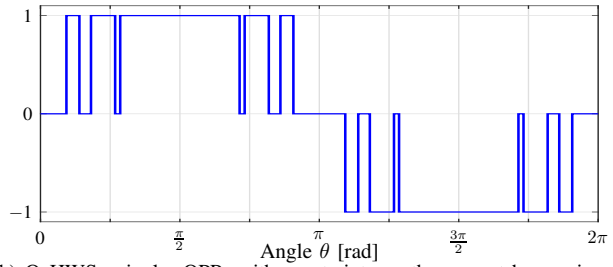

(b) QaHWS unipolar OPPs with constraints on the current harmonics

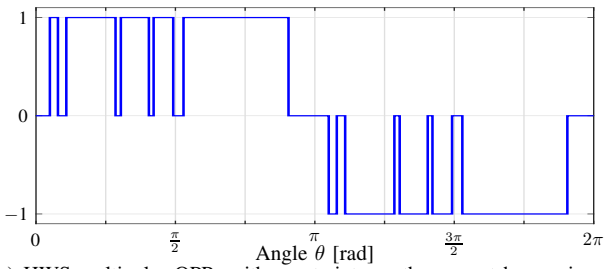

(c) HWS multipolar OPPs with constraints on the current harmonics

Fig. 6. OPPs with $d = 5$ and $m = 1.085$ resulted from the unipolar QaHWS OPP optimization problem (a) without and (b) with constraints on the grid current harmonics, and (c) the current harmonic-constrained HWS multipolar OPP optimization problem.

fact that the OPPs are computed such that *both* the current TDD is minimized, while considering the LCL filter transfer function from the switching signal to the grid current, and relevant harmonics are constrained to comply with the grid standards.

Subsequently, the harmonic spectra of the harmonic-constrained HWS multipolar OPPs are shown in Figs. 7(c) and 8(c) for $m = 1.035$ and $m = 1.085$, respectively. Starting from the latter operating point, as can be seen in Fig. 8(c), the 17^{th} harmonic is well within its limit, while I_{TDD} is as low as 1.86%, i.e., it is lower than that of the constrained QaHWS unipolar OPPs. Similar performance can be observed for $m = 1.035$ (see Fig. 7(c)), where all current harmonics, including the 17^{th}, are relatively low and within their permissible ranges, thus resulting in $I_{\text{TDD}} = 1.37\%$. This value of current TDD is not only lower than that achieved with the constrained QaHWS unipolar OPPs, but it is even lower than that produced with the conventional (unconstrained) OPPs. Finally, it is worth mentioning that the 19^{th} harmonic in Fig. 7(c)—which is limited to its maximum allowed value—reveals the reason why constraints on all relevant low-frequency harmonics are added to the OPP problem, instead of merely imposing constraints on the harmonics that violate their limits in the unconstrained OPP case (e.g., the 17^{th} harmonic in the discussed case).

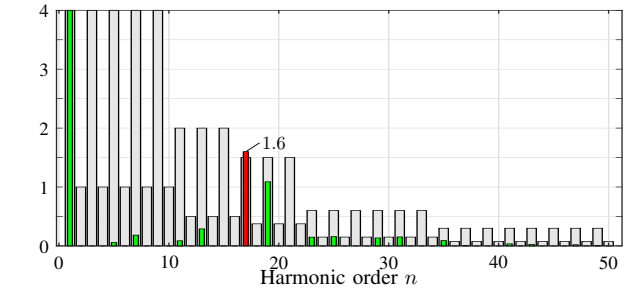

(a) QaHWS unipolar OPPs without constraints on the current harmonics; $I_{\text{TDD}} = 1.41\%$

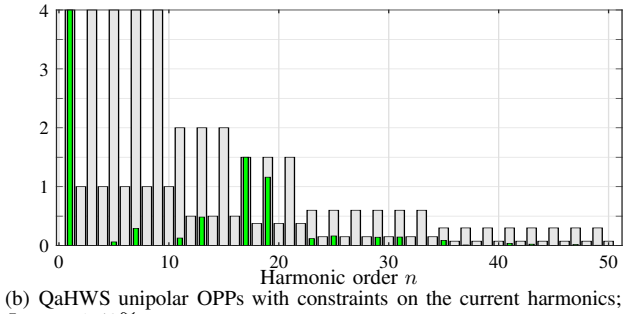

(b) QaHWS unipolar OPPs with constraints on the current harmonics; $I_{\text{TDD}} = 1.42\%$

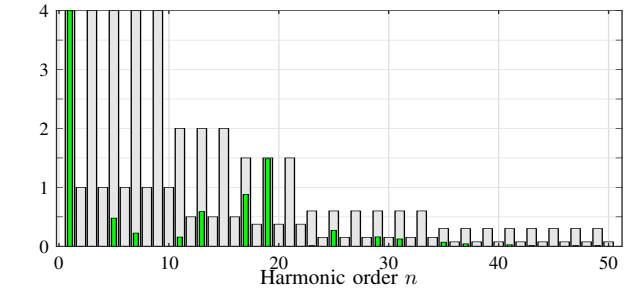

(c) HWS multipolar OPPs with constraints on the current harmonics; $I_{\text{TDD}} = 1.37\%$

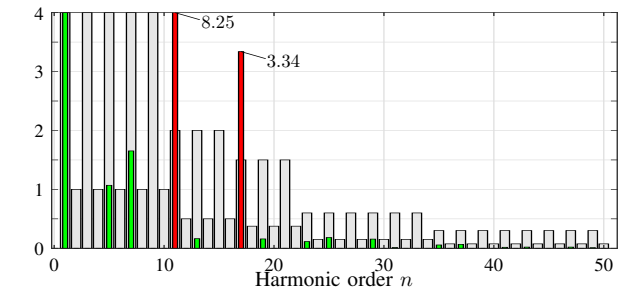

(d) SVM; I_{TDD}=6.45 %

Fig. 7. Grid current harmonics (%) for $m = 1.035$. The grid standard limits are shown as light gray bars, current harmonics that meet them are shown as green bars, while harmonics that violate them are shown as red bars.

In a last step, for comparison purposes, SVM is implemented by means of asymmetric regularly sampled CB-PWM with appropriate common-mode voltage injection [1]. Comparing the current harmonic spectra produced by the constrained OPPs with that of SVM (compare Figs. 7(c) and 7(d), or Figs. 8(c) and 8(d)), it is evident that the latter has much higher harmonic amplitudes, as verified by the 6.45% and 8.36% current TDD for modulation indices $m = 1.035$ and $m = 1.085$, respectively. These values are about five to six times greater than the I_{TDD} achieved with the proposed modulation scheme.

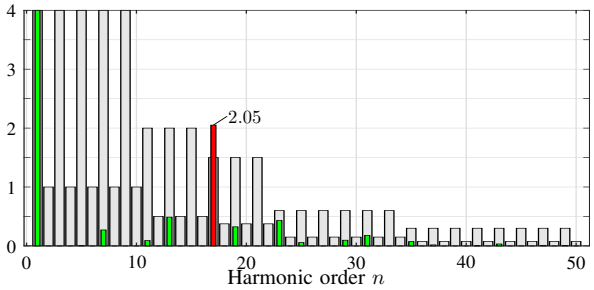

(a) QaHWS unipolar OPPs without constraints on the current harmonics; $I_{\text{TDD}} = 1.56\%$

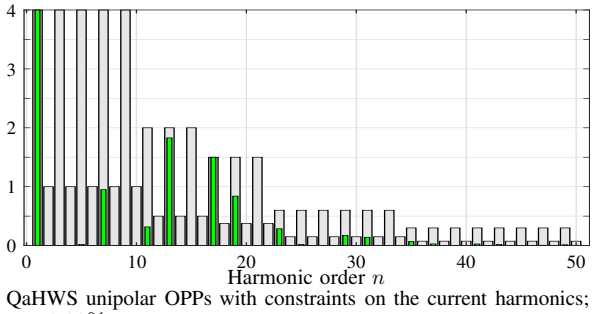

(b) QaHWS unipolar OPPs with constraints on the current harmonics; $I_{\text{TDD}} = 1.93\%$

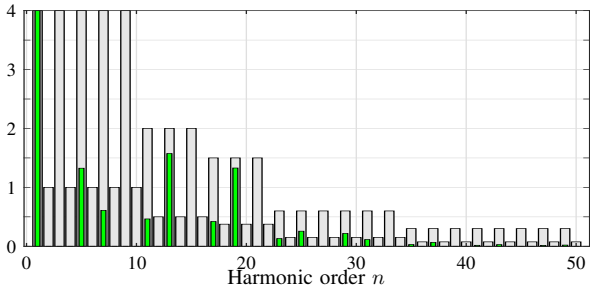

(c) HWS multipolar OPPs with constraints on the current harmonics; $I_{\text{TDD}} = 1.86\%$

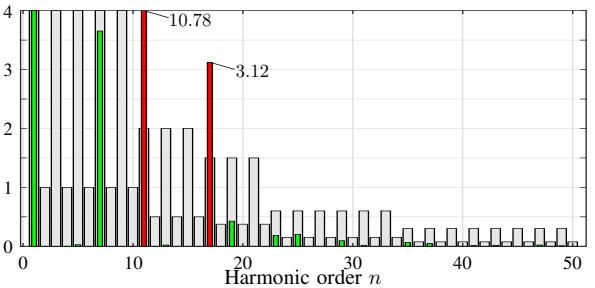

(d) SVM; I_{TDD}=8.36 %

Fig. 8. Grid current harmonics (%) for $m = 1.085$. The grid standard limits are shown as light gray bars, current harmonics that meet them are shown as green bars, while harmonics that violate them are shown as red bars.

Besides, individual harmonics clearly exceed their limits for both studied modulation indices, rendering SVM unsuitable for the specific application. Hence, these results clearly highlight the benefits of the proposed OPPs and their superior harmonic behavior.

IV. Conclusion

This paper presented the computation of three-level OPPs for grid-connected converters with LCL filters. Even though OPPs can produce the theoretical minimum current TDD, they cannot ensure that harmonic grid standards are met when applied to grid-connected power converters. As shown in this work, by minimizing the grid current TDD and constrain individual current harmonic amplitudes, the grid standards can be fully respected, while achieving the best possible harmonic performance. In addition, by relaxing the artificially imposed restrictions on the three-level OPPs, i.e., quarter-wave symmetry and unipolar switch positions, which limit the search space, the computed OPPs can further improve the current quality and achieve an even more favorable harmonic performance. As demonstrated with the presented numerical results, the proposed harmonic-constrained HWS multipolar OPPs not only outperform conventional modulation methods, such as SVM, but they are able to even occasionally produce lower current TDD values than that of conventional (unconstrained) OPPs.

Acknowledgment

This work was supported by the Academy of Finland.

References

[1] D. G. Holmes and T. A. Lipo, *Pulse width modulation for power converters: Principles and practice*. Piscataway, NJ, USA: IEEE Press, 2003.

[2] H. S. Patel and R. G. Hoft, "Generalized techniques of harmonic elimination and voltage control in thyristor inverters: Part I—Harmonic elimination," *IEEE Trans. Ind. Appl.*, vol. IA-9, no. 3, pp. 310–317, May 1973.

[3] G. S. Buja, "Optimum output waveforms in PWM inverters," *IEEE Trans. Ind. Appl.*, vol. IA-16, no. 6, pp. 830–836, Nov./Dec. 1980.

[4] IEEE Std 519-2014 (Revision of IEEE Std 519-1992), "IEEE recommended practices and requirements for harmonic control in electrical power systems," pp. 1–29, Jun. 2014.

[5] J. Pontt, J. Rodriguez, and R. Huerta, "Mitigation of noneliminated harmonics of shepwm three-level multipulse three-phase active front end converters with low switching frequency for meeting standard ieee-519-92," *IEEE Trans. Power Electron.*, vol. 19, no. 6, pp. 1594–1600, Nov. 2004.

[6] A. Moeini, H. Iman-Eini, and M. Bakhshizadeh, "Selective harmonic mitigation–pulse-width modulation technique with variable dc-link voltages in single and three-phase cascaded H-bridge inverters," *IET Power Electron.*, vol. 7, no. 4, pp. 924–932, Apr. 2014.

[7] L. G. Franquelo, J. Nápoles, R. C. P. Guisado, J. I. León, and M. A. Aguirre, "A flexible selective harmonic mitigation technique to meet grid codes in three-level PWM converters," *IEEE Trans. Ind. Electron.*, vol. 54, no. 6, pp. 3022–3029, Dec. 2007.

[8] J. Nápoles, A. J. Watson, J. J. Padilla, J. I. León, L. G. Franquelo, P. W. Wheeler, and M. A. Aguirre, "Selective harmonic mitigation technique for cascaded H-bridge converters with nonequal dc link voltages," *IEEE Trans. Ind. Electron.*, vol. 60, no. 5, pp. 1963–1971, May 2013.

[9] A. K. Rathore, J. Holtz, and T. Boller, "Synchronous optimal pulsewidth modulation for low-switching-frequency control of medium-voltage multilevel inverters," *IEEE Trans. Ind. Electron.*, vol. 57, no. 7, pp. 2374–2381, Jul. 2010.

[10] T. Dorfling, H. d. T. Mouton, and T. Geyer, "Generalized model predictive pulse pattern control based on small-signal modeling—Part 2: Implementation and analysis," *IEEE Trans. Power Electron.*, vol. 37, no. 9, pp. 10 488–10 498, Sep. 2022.

[11] M. Rossi, P. Karamanakos, and F. Castelli-Dezza, "An indirect model predictive control method for grid-connected three-level neutral point clamped converters with LCL filters," *IEEE Trans. Ind. Appl.*, vol. 58, no. 3, pp. 3750–3768, May/Jun. 2022.

[12] T. Geyer, *Model predictive control of high power converters and industrial drives*. Hoboken, NJ, USA: Wiley, 2016.

[13] A. Birth, T. Geyer, H. d. T. Mouton, and M. Dorfling, "Generalized three-level optimal pulse patterns with lower harmonic distortion," *IEEE Trans. Power Electron.*, vol. 35, no. 6, pp. 5741–5752, Jun. 2020.